2021

Super-resolution reconstruction of brain magnetic resonance images via lightweight autoencoder

J. Andrew

T.S.R. Mhatesh

Robin D. Sebastin

K. Martin Sagayam

Jennifer Eunice

See next page for additional authors

Authors

J. Andrew, T.S.R. Mhatesh, Robin D. Sebastin, K. Martin Sagayam, Jennifer Eunice, Marc Pomplun, and Helen Dang

Informatics in Medicine Unlocked 26 (2021) 100713

Contents lists available at ScienceDirect

Informatics in Medicine Unlocked

journal homepage: www.elsevier.com/locate/imu

Super-resolution reconstruction of brain magnetic resonance images via lightweight autoencoder

J. Andrew [a], T.S.R. Mhatesh [b], Robin D. Sebastin [a], K. Martin Sagayam [c], Jennifer Eunice [c], Marc Pomplun [d], Hien Dang [d,e,*]

[a] Department of Computer Science and Engineering, Karunya Institute of Technology and Sciences, Coimbatore, India
[b] Department of Bioinformatics, Karunya Institute of Technology and Sciences, Coimbatore, India
[c] Department of Electronics and Communication Engineering, Karunya Institute of Technology and Sciences Coimbatore, India
[d] Department of Computer Science, University of Massachusetts Boston, MA, USA
[e] Faculty of Computer Science and Engineering, Thuyloi University, Viet Nam

ARTICLE INFO

Keywords:
Super-resolution
MRI
Image enhancement
Autoencoder

ABSTRACT

Magnetic Resonance Imaging (MRI) is useful to provide detailed anatomical information such as images of tissues and organs within the body that are vital for quantitative image analysis. However, typically the MR images acquired lacks adequate resolution because of the constraints such as patients' comfort and long sampling duration. Processing the low resolution MRI may lead to an incorrect diagnosis. Therefore, there is a need for super resolution techniques to obtain high resolution MRI images. Single image super resolution (SR) is one of the popular techniques to enhance image quality. Reconstruction based SR technique is a category of single image SR that can reconstruct the low resolution MRI images to high resolution images. Inspired by the advanced deep learning based SR techniques, in this paper we propose an autoencoder based MRI image super resolution technique that performs reconstruction of the high resolution MRI images from low resolution MRI images. Experimental results on synthetic and real brain MRI images show that our autoencoder based SR technique surpasses other state-of-the-art techniques in terms of peak signal-to-noise ratio (PSNR), structural similarity (SSIM), Information Fidelity Criterion (IFC), and computational time.

1. Introduction

Magnetic Resonance Imaging (MRI) [1] is one of the best approaches to give a precise clinical conclusion and obsessive investigation because of its non-invasive imaging and powerful characteristics. It is used to visualize the anatomical information within the body such as tissues, tumors, muscles, brain, heart, and so on. MRI plays an important role in neurological and brain research. However, spatial and low resolution are persistent problems that MRI often faces that affect the diagnosis process and post-processing [2]. There are many problems faced in medical imaging [3–5]. The tradeoff between high quality MRI images often comes with a long sampling time, patients discomfort, stronger magnetic field, increased expenses. Such things are clinically challenging and rarely possible. To address this problem without changing the scanning protocol or scanning hardware, super resolution (SR) approaches yield promising results. SR approaches are popular in the field of computer vision in the past decades. In recent, much literatures are proposed to enhance the quality of the image [6–8]. SR approaches can be classified into single image super resolution (SISR) and multiple image super resolution (MISR). In SISR, the SR image is recovered from a single LR image. In MISR, the SR image is reconstructed based on the aggregated accuracy of the multiple LR images. This is considered as the main drawback of the MISR method because it is challenging to capture multiple images of the same object and it is clinically impossible due to patients' comfort [9].

SISR [10] methods can be categorized into model-based SR [11], reconstruction-based SR [12], and learning-based SR [13]. Model-based SR techniques use interpolation algorithms such as nearest neighbor, bicubic, and bilinear to reconstruct the HR features from the LR images by estimating the pixel values in the HR grids. Though it yields HR images at high computational efficiency they result in blurred edges, displeasing artifacts, and overly smooth reconstructed images with

* Corresponding author. Faculty of Computer Science and Engineering, Thuyloi University, 175 TaySon Str., DongDa Dist., Hanoi, Viet Nam.
E-mail addresses: andrewj@karunya.edu (J. Andrew), madeshselvarani@gmail.com (T.S.R. Mhatesh), robin.d.sebastian@gmail.com (R.D. Sebastin), martinsagayam.k@gmail.com (K.M. Sagayam), jennifer.onesimu@gmail.com (J. Eunice), marc@cs.umb.edu (M. Pomplun), hiendt@tlu.edu.vn (H. Dang).

https://doi.org/10.1016/j.imu.2021.100713
Received 22 February 2021; Received in revised form 19 August 2021; Accepted 19 August 2021
Available online 28 August 2021

missing fine details. Reconstruction-based SR solves the problem of blurred edges through precise prior knowledge of HR. The HR images are reconstructed based on prior knowledge such as edge, gradient, and global means. However, the reconstructed images lack fine details at high magnification. In learning-based SR models use various machine learning techniques to learn the mapping between SR and LR images. It analyses the HR-LR images pairs and predicts HR features from an LR image. Sparse-coding [14] is one of the learning-based SR methods that yield promising results by assuming that the LR image patch from the dictionary matches the HR image from the HR dictionary. Due to the restrictions and ineffectiveness of this assumption, SR produces unpleasant results. To solve these problems different variants of SR techniques have been proposed recently [8,15–17].

Recently, due to the hasty evolution of machine learning, particularly deep learning (which is a subset of machine learning) models are efficient in extracting the hidden features of an image and it is proven successful in image classification [18]. Inspired by the capability of deep learning, many kinds of literature have been proposed on SR studies. The state-of-the-art literature includes deep learning models such as Convolutional Neural Network (CNN) [19], Generative Adversarial Network (GAN) [20], residual neural network (ResNet) [21], and recurrent neural network (RNN) [22]. Multiple variants of deep learning models are available in the state-of-the-art literature they are Super resolution convolutional neural network (SRCNN) [23], fast super resolution convolutional neural network (FSRCNN) [24], deep recursive convolutional network (DRCN) [25], very deep convolutional networks (VDSR) [19], and super resolution generative adversarial network (SRGAN) [20]. Though these approaches have some success in reconstructing HR natural images, they are not applicable for MRI images. SR approaches for MRI image enhancements are also appeared in the state-of-the-art research [8,15,17,26–28]. However, they produce irrelevant artifacts and distortions. SR approaches for MRI images should deliver relevant artifacts and details that are clinically pertinent. Hence, the challenges to develop an SR approach for MRI images are clear as the existing approaches do not satisfy all the requirements and it is obligatory to develop a new SR approach.

Autoencoder [29] is an unsupervised deep learning model that can learn the representation of the images. In recent autoencoder based SR has been proposed [30–32]. The autoencoder based SR models are yielding promising results with reduced computational complexity. Autoencoder is a combination of encoder and decoder. The encoder learns the input images and translates them into a latent space representation. The decoder reconstructs the image only from the latent space representation. Dong et al. [14] proposed sparse coding based SR model. Sparse coding assumes that the sparse representation of HR image from HR dictionary is similar to LR image patch from LR dictionary. Sparse representation noise is proposed to overcome this assumption by employing non local means where the HR representations can be estimated from LR representations. Other authors such as Wang et al. [33], Yang and Yang [34], Chang et al. [35], Shao et al. [31], Park et al. [30], proposed similar SR approaches based on sparse and auto encoder based SR approaches. However, mostly they use the dictionary training method where the LR image patch can be considered as HR image patches either directly or through estimations. Also, it is hard for simple linear mapping to represent complex relationships, this is another major limitation of the existing study.

In this paper, an autoencoder based SR model is presented for MRI. The presented model takes an LR MRI image and input and reconstructs the corresponding HR image. Conceptually, the autoencoder generates the output image of the same dimension as input from the latent space representation generated by the encoder. In the proposed model, the autoencoder reconstructs the HR MRI slices from the LR MRI slices based on the scaling factor. It consists of feature extraction, nonlinear mapping, and reconstruction steps. The efficiency of the proposed SR model is evaluated based on Mean Squared Error (MSE), Peak Signal to Noise Ratio (PSNR), Structural Similarity Index (SSIM) [36], Information Fidelity Criterion (IFC), and computational time.

The remainder of this paper is organized as follows. The state-of-the-art literature proposed on single image SR is presented in section 2. The proposed modified autoencoder based SR is discussed in section 3. Section 4 presents the experiments carried out, the dataset details, experimental analysis, and performance evaluation. Finally, section 5 concludes.

2. Related works

2.1. Image super-resolution using deep learning

In recent, deep learning based SR approaches have seen a rise in the literature. Artificial Neural Networks (ANN), CNN, GAN are some of the popular deep learning based SR approaches. ANN based SR approach has emerged in 2006 [37]. However, in recent CNN based SR approaches have been paid more attention by researchers. SRCNN [23] is one of the first CNN based SR in the literature. Subsequently, different variants of methods are proposed by modifying the depth and the hyperparameters to achieve state-of-the-art performance. FSRCNN [24] is one of the approaches that yield high SR image restoration accuracy with a simple network structure. Kim et al. proposed VDSR [19] and DRCN [25] with increased network depth and achieved better performance than SRCNN.

SRGAN [20] is a generative adversarial network (GAN) based SR approach proposed by Ledig et al. This is the first framework to reconstruct photo-realistic SR using GAN. To achieve this perceptual loss function along with L2 loss function has been used. Lim et al. [38] have proposed a method called Enhanced Deep Super-Resolution Network (EDSR). It achieved better performance than other state-of-the-art SR approaches. It reduced the number of layers in the conventional residual networks. When the model size is expanded the performance is further improved. To reconstruct high-resolution images of different up-scaling factors in a single model a new technique called Multi-scale Deep Super Resolution system (MDSR) [39] is proposed. It uses wavelet coefficients along with CNN to reconstruct the SR images. Along with, residual neural networks (ResNet) [40], recurrent neural network (RNN) [22], and DenseNet [41] are other effective SR approaches. Tong et al. [42] have proposed an image SR approach based on ResNet with skip connections. Zhang et al. [43] proposed a dense ResNet to achieve state-of-the-art performance over CNN based approaches. Tai et al. [44] reduced the parameter burden of the deep learning model by reusing the parameters through recursive blocks. Hu et al. proposed a cascaded multiscale cross network (CMSCN) to acquire more information to reconstruct the HR images. These approaches have been successful to some extent on natural image processing (NIP) tasks.

2.2. MRI image super resolution

Due to the success of SR approaches in NIP deep learning based SR methods have also been proposed to the MR imaging fields. CNN and GAN based SR approaches have been widely used in MRI SR. A CNN based SR approach for brain MRI is proposed by Bahrami et al. [45]. The model takes anatomical labels of brain tissues and intensity as the input to reconstruct MRI SR. Enhanced Deep Residual Network (EDRN) [38] is proposed by Zhao et al. to enhance the synthetic multi-orientation of brain MRI images through ResNet. Chen et al. [46] proposed a 3D densely connected super resolution network (DCSRN) to reconstruct the HR features of brain MRI using neural network architecture. Mane et al. [24] proposed an FSRCNN based 3D CNN to reconstruct the high-dimensional features of MRI images. It lacks a balance between the MRI quality and computational complexity. As the network gets deeper there is an increase in complexity. Özyurt et al. [47] proposed a fuzzy C means SR CNN approach to segment the brain MRI images with high quality features. This approach used pretrained network squeezeNet. GAN based SR approach is proposed by Lyu et al. [27] where the MRI images are enlarged using commonly used SR algorithms and GAN is

trained and generates SR MRI images. Then ensemble learning method is utilized to finalize the SR images. Ebner et al. [48] have proposed an SR reconstruction framework for fetal brain MRI based on CNN based network.

A dilated convolutional encoder-decoder (DCED) network has been proposed in Ref. [28] to improve the resolution of MRI by extracting high resolution features through the enlarged receptive field without increasing the parameters or layers. By enlarging the receptive field, dilated encoders capture wider information. To decode the information, a deconvolution operation is used in grinding artifacts and storing fine details. The input image information loss caused by CNN's pooling layer is addressed by the work Park et al. [30]. An autoencoder based CNN image super resolution model is proposed with a deconvolutional layer. This method achieved substantial state-of-the-art performance in terms of PSNR, SSIM, and computational time. Xue et al. [8] proposed a progressive sub-band residual learning SR network to improve the spatial resolution of MRI images. This model used two parallel learning streams, they are to learn the missing high residuals and to reconstruct the MRI image. Zhao et al. [49] proposed a channel splitting network SR approaches that divide the hierarchical features of MRI images into the residual and dense branch. The residual branch identifies the features to reuse and the dense branch explores the new features.

From the above literature study, it is understood that the image super-resolution has acquired a lot of attraction in recent times. It is observed that deep learning based SR techniques are predominant. It is also inferred that various state-of-the-art deep learning based SR approaches have been proposed and they are successful to some extent. However, such a model lacks a proper training dataset and has been trained with different or ensemble datasets. Table 1 shows some of the popular SR approaches and their specifications.

3. Materials & methods

The main objective of this study is to reconstruct HR MRI with extrapolated signals. The original size of the MRI images is 240 X 240 and 256 X 256 that is reconstructed based on scaling factors. The scaling factor determines the magnification power (for example, if a scaling factor is 2 then the resolution of the original image is enlarged 2 times than the actual size). MRI images are information rich as they can detect tumors, systs, infections, blood vessels, etc. While magnifying an original MRI image, the image quality decreases since the original MRI does not have adequate spatial resolution information. However, edges in upsampled (i.e., magnified) images are adequately sharp. LR images cannot be neglected with blurring effects. Downsampling methods produce blurry or pixelated images. Bicubic interpolation is one of the techniques that blur the image with a downscaling factor of '2', with a 3x3 average filter along with nearest neighbor interpolation. Hence, the bicubic blurring and pixel information loss is given as:

$$I_{LR} = D^{f}_{bicubic}(I_{HR}) \tag{1}$$

Where I_{LR} represents LR MRI images and I_{HR} for its corresponding HR image. $I_{LR} \in R^n$ and $I_{HR} \in R^m$ $(m > n)$. R^n& R^mrepresents the image resolution. $D^{f}_{bicubic}$ represents the downsampling of bicubic interpolation with scaling factor f. The proposed autoencoder based SR Algorithm aims to adjudge I_{HR} from I_{LR}. The recovery of I_{HR} from I_{LR} is an inverse problem where it is fairly possible to obtain different results of I_{HR} for a given I_{LR}. The autoencoder based SR is trained to reconstruct the image from I_{LR} it can be achieved when the model loss is minimized considerably. The loss function can be defined as an optimization problem, shown in equation (2).

$$I'_{HR} = argmin_{I_{HR}} \left|\left|I_{LR} - D^{f}_{bicubic}.I_{HR}\right|\right|^2 \tag{2}$$

Where I'_{HR} is the reconstructed image obtained by minimizing the loss function. The notations $\left|\left|I_{LR} - D.I_{HR}\right|\right|^2$ represents the $L2$ regularization.

The output I_{HR} can be defined as,

$$I_{HR} = F(X; f; \theta) \tag{3}$$

Where F denotes proposed SR functions latent space representation, θ represents the parameter set such as weights and biases for the function and X represents the local features of the input LR MRI.

3.1. Proposed autoencoder based SR

Autoencoder based SR approach consists of an autoencoder that takes I_{LR} as input and produces the corresponding I_{HR} based on the scaling factor. Fig. 1 shows the architecture diagram of the autoencoder based SR. In addition to the regular autoencoder, the proposed autoencoder model consists of convolution layers and activation functions for feature extraction, and a deconvolution layer for reconstruction. The visualization of the proposed SR autoencoder network with skip connections is shown in Fig. 2. In the network model, pooling layers have not been used as it cause information loss when it selects the features and reduces the parameters. The deconvolution layer at the end of the network is used to upsample the input MRI image and to reconstruct the MRI from the latent space representation.

Autoencoder is a combination of encoder and decoder. The function of the encoder and decoder is given as:

$$\varphi : X \rightarrow F$$

$$\psi : F \rightarrow X$$

$$\varphi, \psi = \arg_{\varphi,\psi}\min \left|\left|X - X'\right|\right|^2 \tag{4}$$

Where φ and ψ represents the encoder and decoder functions, X represents the input I_{LR} and F represents the latent space representation. Equation (4) shows the loss function of the autoencoder function where X' represents the reconstructed image I_{HR}. The hidden layer

Table 1
Comparison of State-of-the-art SR approaches.

Reference	SR Approach	Input	Upsampling	Technique	Loss Function	Reconstructions
Dong et al. [23]	SRCNN	Natural Images	Bicubic	CNN	L2 (MSE)	Direct
Kim et al. [25]	DRCN	Natural Images	Bicubic	CNN	L2	Direct
Dong et al. [24]	FSRCNN	Natural Images	DeConv	CNN	L2	Direct
Kim et al. [19]	VDSR	Natural Images	Bicubic	CNN	L2	Direct
Ledig et al. [20]	SRGAN	Natural Images	Sub-pixel	GAN	L2 + Perceptual loss	Direct
Lim et al. [38]	EDSR	Natural Images	Sub-pixel	ResNet	L1	Direct
Han et al. [63]	DSRN	Natural Images	DeConv	RNN	L2	Progressive
Shao et al. [31]	CSAE	Remote sensing images	Bicubic	Coupled Sparse autoencoder	L1	Direct
Park et al. [30]	ACNS	MRI	Bicubic	Autoencoder inspired CNN	MSE	Direct
Pham et al. [61]	DCNN-SCSR	MRI	Sub-pixel	Autoencoder	L2	Direct
Xue et al. [8]	PSR-SRN	MRI	Bicubic	ResNet	MSE	Progressive
Zhao et al. [49]	CSN	MRI	Bicubic	ResNet and DenseNet	L1 & L2	Direct
Lyu et al. [27]	ELSR	MRI	Bicubic	Ensemble learning	MSE	Direct

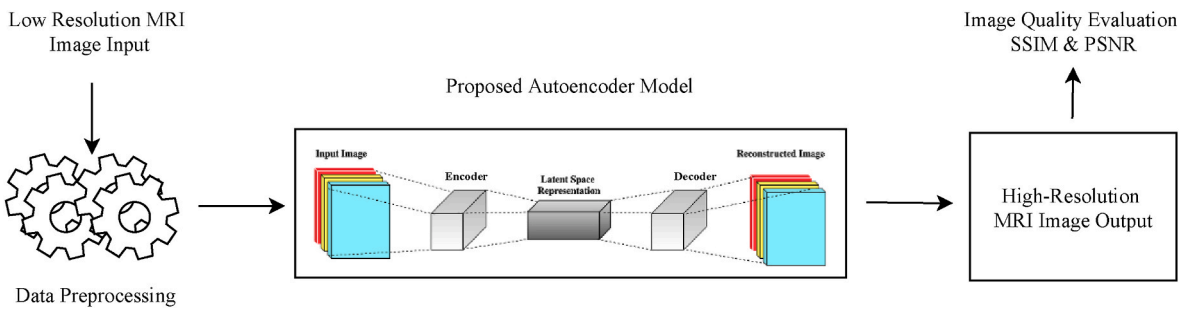

Fig. 1. The architecture of Proposed SR Autoencoder.

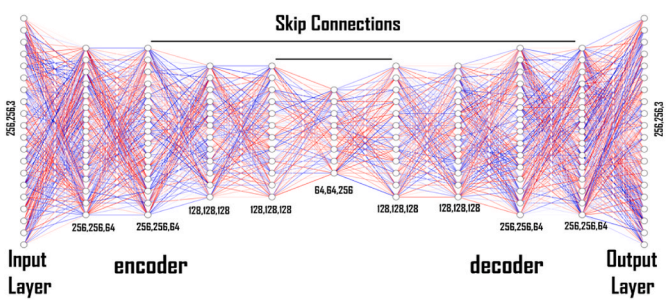

Fig. 2. Visualization of SR autoencoder network with skip connections.

functionalities are represented as:

$$F = f(W.X + b) \tag{5}$$

$$X' = f(W'.F + b) \tag{6}$$

F denotes the latent space representation of the input I_{LR} image. Equations (4) and (5) represents the hidden layer functions. An activation function defines the output of every layer in the network. In the proposed SR autoencoder "ReLu" activation function is used for every layer along with the optimizer "Adam".

$$R(z) = \max(0, z) \tag{7}$$

Equation (6) shows the activation function "ReLu" it is denoted as $R(z)$.

following equation.

$$F_1 = \max(W_1.X + B_1, 0) + \alpha \min(W_1.X + B_1, 0) \tag{8}$$

where convolution operation is represented as '. ', max () and min () represents activation function, W_1 represents filters and B_1 represents biases.

The non-linear mapping between I_{LR} and I_{HR} is given as follows:

$$\sum_{i=1}^{n} F_i(X_i) = \max(W_i + X_i + B_i, 0) + \alpha \min(W_i + X_i + B_i, 0) \tag{9}$$

where F_i, X_i, W_i and B_i indicates the non-linear mapping of ith recurrence.

After the feature extraction and non-linear mapping, the obtained HR features are given to a deconvolution operation to reconstruct the HR MRI based on the scaling factor and obtained HR feature aggregate. It is represented as follows:

$$\sum_{i=1}^{n} F_{i+f}(X_{i+f}) = deconv(X_{i+f} + W_{i+f} + B_{i+f}) \tag{10}$$

where *deconv()* represents the deconvolution operation, and F_{i+f}, X_{i+f}, W_{i+f}, and B_{i+f} denotes the parameters with scaling factor f. The overall operation of the proposed system is summarized in the following Algorithm.

Algorithm. Autoencoder Based SR

Algorithm : Autoencoder Based SR

Input: I_{LR} MRI; f - scaling factor; n - number of iterations, θ - weights and biases
Output: I'_{HR} - reconstructed HR image
1: Feature extraction from input I_{LR} with θ by equation (8)
2: **for** i=1 to n **do**
3: perform non-linear mapping to the extracted features using equation (9)
4: **end for**
5: HR feature acquisition using equation (9)
6: Reconstruct I'_{HR} based on scaling factor f and aggregated HR features with equation (10)

The proposed autoencoder based SR approach consists of feature extraction, non-linear mapping, and reconstruction. The local features of I_{HR} are extracted based on the receptive fields. It is described using the

3.2. Performance metrics

The proposed autoencoder based SR training is focused to obtain the

optimal θ with a minimal loss between original I_{HR} and reconstructed I'_{HR}. It is calculated by mean square error (MSE) [50]. To evaluate the performance of the proposed SR study, we used typical SR study metrics, which are peak signal-to-noise ratio (PSNR) [51], structural similarity index (SSIM) [52] and information fidelity criterion (IFC) [53].

The loss metric MSE is calculated to understand the difference in linking the reconstructed MRI image and the target image super-resolution. The MSE loss metric can be represented as:

$$L_{SR}^{MSE} = \frac{1}{MN}\sum_{n=1}^{M}\sum_{m=1}^{N}\left[I'_{HR}(n,m) - F\left(I_{HR}(n,m)\right)\right]^2 \tag{11}$$

where n, m are the pixel dimensions of the image. L_{SR}^{MSE} calculates the MSE pixel wise for the original HR MRI image and the reconstructed SR MRI image from the LR MRI image.

SSIM is a performance metric used to calculate the reconstructed image quality. SSIM is developed by Wang [36], to quantify the quality degradation of the reconstructed image. The structural quality of the reconstructed SR image is given by

$$SSIM = \frac{(2\mu_s\mu_{SR} + C_1)(2\sigma_{SSR} + C_2)}{\left(\mu_s^2 + \mu_{SR}^2 + C_1\right) + \left(\sigma_S^2 + \sigma_{SR}^2 + C_2\right)} \tag{12}$$

μ and σ denotes mean and standard deviation respectively. C_1 and C_2 are constants introduced to the formula for stabilization. The SSIM value would be 1 if the reconstructed SR MRI image and HR MRI image are identical.

PSNR computes the decibels of the peak signal-to-noise ratio between the actual and reconstructed SR images. The higher values of PSNR denote the better quality of the reconstructed SR image. The PSNR value can be calculated by equation (13)

$$PSNR = -10log_{10}\frac{e_{MSE}}{S^2} \tag{13}$$

IFC computes the mutual information between the original MRI and the reconstructed HR MRI.

$$IFC = \sum_{k\in subbands} I\left(C^{N_k,k}; N^{N_k,k}\middle|s^{N_k,k}\right) \tag{14}$$

where N_k denotes coefficient of k subbands for $C^{N_k,k}$, $N^{N_k,k}$, and $s^{N_k,k}$.

3.3. Dataset details

The proposed SR autoencoder has experimented on multimodal brain tumor segmentation challenge (BraTS2017) [54–56] and MRBrain18 [57]. BraTS2017 consists of 285 MRI images of resolution 256 × 256 x 3. It comprises four modal brain MRI scans such as T1, T1-weighted, T2-weighted, and T2 FLAIR. We selected 200 MRI images slices of T1 and T2 FLAIR. MRBrain18 consists of T1, T1-IR, and T2-FLAIR. We selected 31 MRI slices for experimentation. The dimension of MRI images of MRBrain18 is 240 X 240. Fig. 3 shows the sample MRI images from BraTS2017 and MRBrain18. Table 2 summarizes the dataset used in the experiment.

Table 2
Dataset details.

Dataset	Image Properties	Image Count	Training set	Testing set
BraTS2017 [54]	T1 and T2 Flair 256 × 256 x 3	200	170	30
MRBrain18 [57]	T1 and T2 Flair 240 × 240	31	26	5

4. Experiments & results

In this section, dataset details, experimental configurations, experimental analysis, and performance evaluation of the proposed SR autoencoder is presented.

4.1. Training

The proposed SR autoencoder model has been trained by considering the original MRI images as the ground truth. The LR images are generated from the original MRI images using equation (1). Our model was individually trained and experimented on the two public datasets. The scaling factor has been chosen as '2'. Hence, the resolution of the original MRI images is downscaled from 256 X 256 to 128 X 128 and from 240 X 240 to 120 X 120. The dataset is divided into 85% and 15% for training and testing respectively.

The experiments are carried out in GoogleColab Tesla K80 GPU, and 16 GB RAM. The SR autoencoder model configured with Adam optimizer with learning rate of 0.001, $\beta1 = 0.9$ and $\beta2 = 0.99$ values.

4.2. Experimental analysis

The proposed SR autoencoder model training loss is calculated using equation (11). The model loss is minimized through backpropagation. The network is trained for 1500 epochs approximately. The model achieved minimal MSE loss without overfitting.

Then the model is tested with the 15% of test data. Some random sample input and output of the test data is illustrated in Fig. 4 (a) is the downsampled LR MRI image, Fig. 4 (b) is reconstructed or upsampled MRI image, and Fig. 4 (c) is the ground truth MRI image i.e., the original MRI image.

The model is further tested with random images from the dataset. The MSE values are calculated under the pixel quality difference between the input and the reconstructed SR image output. Fig. 5. Illustrates the model testing with random dataset images.

The MSE value is the divergence between the actual image and the reconstructed SR image. In Fig. 5. (a) the left hand side image is the reconstructed MRI image and the right hand side image is the original

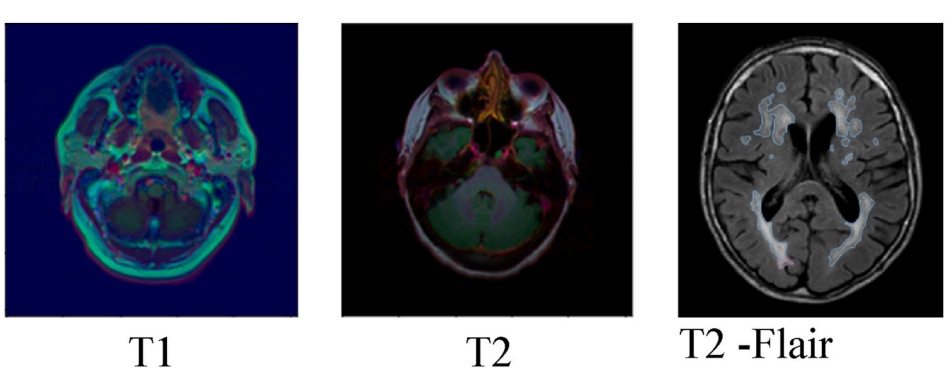

Fig. 3. Sample MRI images from the dataset.

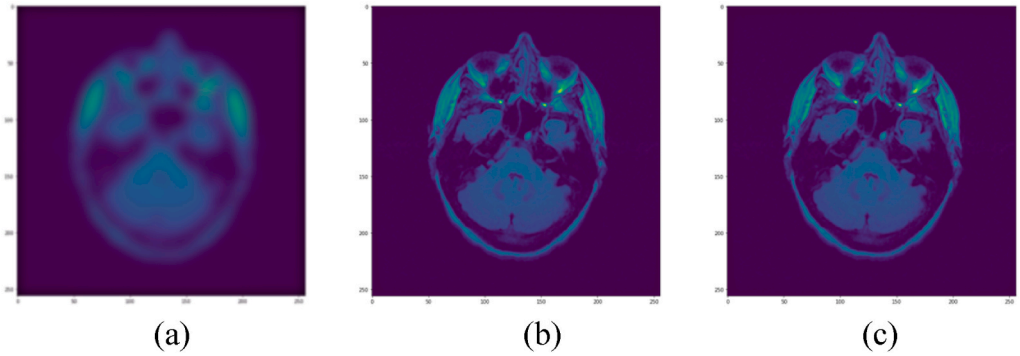

Fig. 4. Experimental results of proposed SR Autoencoder (a) Input: downscaled brain MRI image (b) Output: Reconstructed SR brain MRI image (c) Original HR brain MRI image.

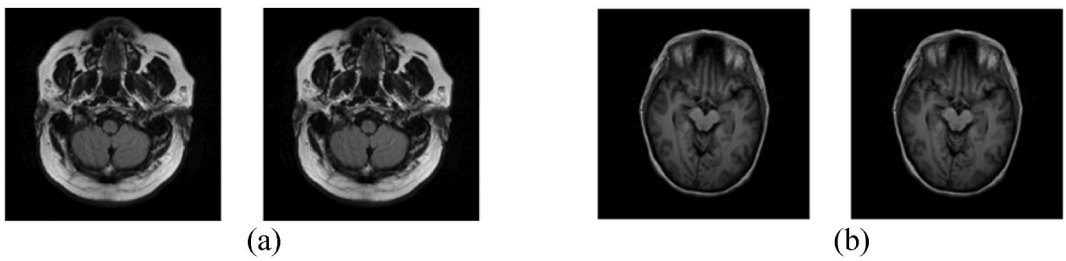

Fig. 5. Model testing. (a) Mse = 0.05 and SSIM = 1.00 (b) MSE = 0.04 and SSIM = 0.99.

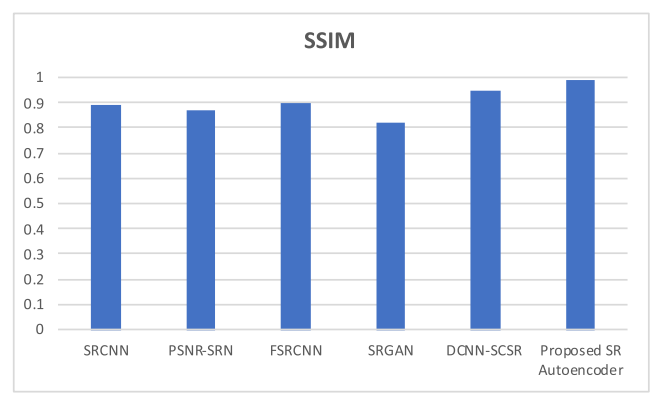

(a)

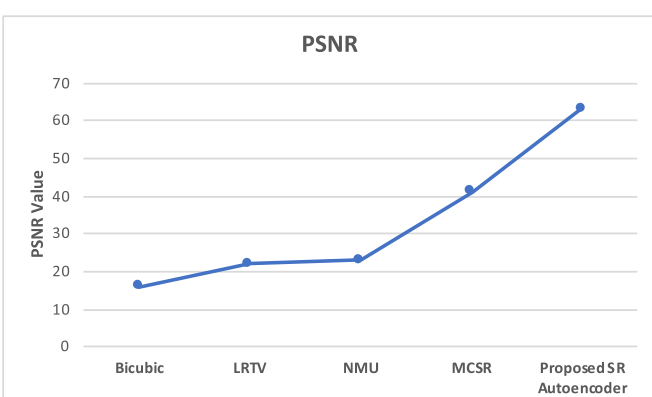

(b)

Fig. 6. Performance evaluation: (a) Comparison of SSIM values with state-of-the-art approaches, (b) Comparison of PSNR values with state-of-the-art approaches.

MRI image. The MSE value between the image is 0.05 and the structural similarity value is 1. This shows that the model generated the SR image identical to the actual HR image. Fig. 5. (b) shows a similar type of SR and original image where the MSE value is 0.04 but the SSIM value is 0.99. This indicates that the model reconstructed a highly similar image with original qualities.

4.3. Performance evaluation

The proposed SR Autoencoder model is compared with state-of-the-art approaches: SRCNN [23], FSRCNN [24], DRCN [25], SRGAN [20], Bicubic [58], LRTV [59], NMU [60], ACNS [30], DCNN-SCSR [61], PSR-SRN [8] and MCSR [62]. The approaches are a combination of model-based and deep learning-based SR. The approaches are compared concerning the SSIM values. Fig. 6 shows the comparison graph of SSIM values of different state-of-the-art approaches.

From Fig. 6. (a) The proposed SR Autoencoder performs better compared with other state-of-the-art approaches. The proposed model achieves a higher SSIM value of 0.99 which is comparatively higher than other approaches. PSNR is the other metric used to evaluate the model. The average PSNR value of the proposed model is 63. Fig. 6. (b) shows the average PSNR value comparison with other approaches. The proposed model is performing better than other approaches.

We further evaluated the performance of the proposed SR autoencoder with the MRBrain18 dataset. Our proposed model achieved better

Table 3
Results of state-of-the-art SR approaches on MRBrain18 dataset.

Approaches	PSNR	SSIM	IFC
SRCNN [23]	26.905	0.846	1.974
Bicubic [58]	22.458	0.688	0.762
NLM [64]	26.318	0.827	2.065
ScSR [65]	26.078	0.821	1.586
VDSR [19]	27.283	0.8571	2.137
LapSR [66]	27.700	0.860	2.067
PSR-SRN [8]	28.067	0.872	**2.307**
Proposed SR Autoencoder	**29.023**	**0.884**	2.301

Table 4
Running time comparison.

Approach	Scaling factor	Time (s)
SRCNN	2	1.59
FSRCNN	2	1.96
DRCN	2	9.06
Proposed SR autoencoder	2	**0.32**

PSNR and SSIM values compared to the state-of-the-art SR approaches on the MRBrain18 dataset. The IFC value our model achieved is also better than most of the approaches. Table 3 shows the comparative analyses of the results. The results used to evaluate the proposed approach are the results obtained on the test dataset.

The proposed model performance is also evaluated based on running time. Table 4 shows the comparison of running time of approaches such as SRCNN, FSRCNN, and DRCN. The running time is taken based on the BraTS 17 dataset with scaling factor '2'. Our approach is fastest compared to the other approaches this proves that the proposed approach is lightweight.

5. Discussion

The major objective of this paper is to reconstruct a HR MRI from a single low resolution MRI. To achieve that an autoencoder based SR approach for MRI images is presented in this paper. The SR autoencoder is proficient of reconstructing HR MRI from LR MRI latent space representation. The proposed yielded better performance with respect to PSNR, SSIM and IFC and also the lightweight nature of the architecture reduced the computational complexity compared to recent state-of-the-art approaches. The network architecture of the proposed approach is simple and uses less number of parameters. The network architecture of the proposed approach is determined through experiments and the details are available in section 3. The architecture provides a balance between the MRI image quality and the computational complexity. The number of parameters used in our approach is 5480 whereas the other state-of-the-art approaches such as SRCNN and FRCNN have used 8032 and 12,464 respectively which are 2 or 3 times greater than the proposed approach. The reduction in the number of parameters minimizes the computational complexity. When the number of layers in the network architecture increases it increases the number of parameters that makes the network training cumbersome. Though, the number of parameters are less compared to other approaches, the performance of the approach is superior due to its suitable network structure. Table 4 compares the running time of the proposed approach for its corresponding scaling factors. It is evident that DRCN takes longer time to calculate the result it is because of deep nature of the network. The network architecture of DRCN has 18 layers and 1,774,080 parameters. Though SRCNN has the shallowest network architecture with only 3 layers, due to its intra layer design it required longer running time. Hence, our proposed network architecture has 6 layers and reduced number of parameters and found to be superior in terms of running time without compromising the image quality.

Further, the performance of the proposed autoencoder based SR approach is evaluated based on the standard performance metrics to measure the quality of the images such as PSNR, SSIM and IFC. Our approach achieved the best PSNR value of 63 compared other state-of-the-art approaches that used similar dataset for experiments. Fig. 6 shows the comparison of SSIM and PSNR values achieved by different state-of-the-art approaches. The performance metrics values shows that the proposed approach has reconstructed the MRI image with adequate details. The reason behind this is the learning ability of the autoencoder in the network architecture. The autoencoder model learned the latent space representation from the input MRI image. The resultant images are then reconstructed based on the latent space representation code. The deconvolution layer at the end of the network architecture reconstructs the MRI image from the features extracted by the convolutional layers and the latent space representation. The proposed approach is experimented with two public real datasets (BraTS2017 and MRBrain18). Fig. 4 shows step-by-step process of the proposed approach. Fig. 4 (a) shows the downscaled and blurred image which lacks appropriate details from the MRI image and given as input to the deep learning network. Fig. 4 (b) is the reconstructed MRI image from the given input MRI image. Fig. 4 (c) is the corresponding original MRI image from the dataset. The reconstructed image is then compared with the original image and the performance metrics values are calculated. Fig. 5 shows the testing of random images from the dataset. The SSIM values are almost 1.00 that shows that there is no loss in the reconstructed image compared to the original image. Also the MSE values is at the lowest proves that there is very minimal error. The overall performance of the proposed approach is presented in Fig. 6 and Table 3. It shows that the proposed approach is having an edge over other state-of-the-art approaches.

Our proposed autoencoder based SR approach has the potential to reduce the MRI sampling time and still achieve higher image quality. It gives patients' comfort as the scan time is not required to be longer but still the we get the higher image quality with adequate structural details. The current work is limited to 2D MRI slice reconstruction. The proposed approach does not consider 3D MRI image features such as structural and spatial information. We are actively working on this as our future direction of this study.

In the experiments, we noticed that the performance of the model is not based on the filters, padding, or number of layers but based on its combination. We also experimented our model with a deep autoencoder model with multiple layers but it cannot achieve better image quality. However, we observed that the performance of any deep learning based SR approach is affected by training. Hence, it gives us a warning that such deep learning models should be used with caution especially in the field of medical imaging.

6. Conclusion

High resolution (HR) MRI images are essential to provide more detailed information for clinical diagnosis. However, it is challenging due to patients discomfort, long sampling time and poor signal-to-noise ratio. To address the aforementioned challenges, we presented an autoencoder based super resolution approach for MRI images to reconstruct the missing structural details of the MRI images through the non-linear mapping between the low resolution (LR) MRI images and HR features and the latent space representation of the LR images. The proposed autoencoder based SR approach has experimented on publicly available BraTS2017 and MRBrain18. Experimental results show that the proposed approach not only outperforms the state-of-the-art SR approaches in terms of PSNR, SSIM, and IFC but also with reduced computational complexity. Additionally, we analyzed the performance of the approach concerning the number of deep learning parameters. The proposed approach uses fewer parameters compared to the state-of-the-art approaches such as SRCNN, FSRCNN, and DRCN and proved to be lightweight without compromising the image quality. Hence, the proposed approach can be used for real time HR MRI reconstruction. However, we noticed that the performance of the deep learning models is directly proportional to the quality of the training set.

This study is limited to 2D in-plane resolution MRI enhancement. In the future, our work aims to enhance 3D MRI images considering the magnitude and phase of the images.

Declaration of competing interest

The authors declare that they have no known competing financial interests or personal relationships that could have appeared to influence the work reported in this paper.

Acknowledgement

We would like to thank all of our universities for facilitating our time support in this paper.

References

[1] Ogawa S, Lee TM, Kay AR, Tank DW. Brain magnetic resonance imaging with contrast dependent on blood oxygenation. Proc. Natl. Acad. Sci. U.S.A Dec. 1990; 87(24):9868–72. https://doi.org/10.1073/pnas.87.24.9868.

[2] Lyu Q, You C, Shan H, Wang G. Super-resolution MRI through deep learning. 2020. arXiv. Oct. 15, 2018, Accessed: May 13, http://arxiv.org/abs/1810.06776.

[3] Andrew Onesimu J, Karthikeyan J. An efficient privacy-preserving deep learning scheme for medical image analysis. Special Issue: The Importance of Human Computer Interaction: Challenges, Methods and Applications J Inf Technol Manag Dec. 2021;12:50–67. https://doi.org/10.22059/jitm.2020.79191.

[4] Andrew J, Fiona R, Caleb Andrew H. "Comparative study of various deep convolutional neural networks in the early prediction of cancer," in *2019 International Conference on Intelligent Computing and Control Systems*. ICCS 2019; May 2019. p. 884–90. https://doi.org/10.1109/ICCS45141.2019.9065445.

[5] Andrew J, DIvyavarshini M, Barjo P, Tigga I. Spine magnetic resonance image segmentation using deep learning techniques. in 2020 6th International Conference on Advanced Computing and Communication Systems ICACCS 2020:945–50. https://doi.org/10.1109/ICACCS48705.2020.9074218. Mar. 2020.

[6] Watanabe A, Furukawa H. Super-resolution technique for high-resolution multichannel Fourier transform spectrometer. Opt Express Oct. 2018;26(21): 27787. https://doi.org/10.1364/oe.26.027787.

[7] Park J, Hwang D, Kim KY, Kang SK, Kim YK, Lee JS. Computed tomography super-resolution using deep convolutional neural network. Phys Med Biol Jul. 2018;63 (14). https://doi.org/10.1088/1361-6560/aacdd4.

[8] X. Xue, Y. Wang, J. Li, Z. Jiao, Z. Ren, and X. Gao, "Progressive sub-band residual-learning network for MR image super resolution," IEEE J. Biomed. Heal. Informatics, vol. 24, no. 2, pp. 377–386, Feb. 2020, doi: 10.1109/JBHI.2019.2945373.

[9] Freedman JN, et al. Super-resolution T2-weighted 4D MRI for image guided radiotherapy. Radiother Oncol Dec. 2018;129(3):486–93. https://doi.org/10.1016/j.radonc.2018.05.015.

[10] Glasner D, Bagon S, Irani M. Super-resolution from a single image. in *Proceedings of the IEEE International Conference on Computer Vision* 2009:349–56. https://doi.org/10.1109/ICCV.2009.5459271.

[11] Zhou F, Yang W, Liao Q. Interpolation-based image super-resolution using multisurface fitting. IEEE Trans Image Process Jul. 2012;21(7):3312–8. https://doi.org/10.1109/TIP.2012.2189576.

[12] Lin Z, Shum HY. Fundamental limits of reconstruction-base superresolution algorithms under local translation. IEEE Trans Pattern Anal Mach Intell Jan. 2004; 26(1):83–97. https://doi.org/10.1109/TPAMI.2004.1261081.

[13] Tang Y, Yan P, Yuan Y, Li X. Single-image super-resolution via local learning. Int. J. Mach. Learn. Cybern. Mar. 2011;2(1):15–23. https://doi.org/10.1007/s13042-011-0011-6.

[14] Dong W, Zhang L, Shi G, Li X. Nonlocally centralized sparse representation for image restoration. IEEE Trans Image Process 2013;22(4):1620–30. https://doi.org/10.1109/TIP.2012.2235847.

[15] Ramanarayanan S, et al. MRI super-resolution using laplacian pyramid convolutional neural networks with isotropic undecimated wavelet loss. In: Proceedings of the annual international conference of the IEEE engineering in medicine and biology society, EMBS. 2020-July; Jul. 2020. p. 1584–7. https://doi.org/10.1109/EMBC44109.2020.9176100.

[16] Cheng R, et al. Automatic magnetic resonance prostate segmentation by deep learning with holistically nested networks. J Med Imaging 2017;4(4):1. https://doi.org/10.1117/1.jmi.4.4.041302.

[17] Mane V, Jadhav S, Lal P. Image super-resolution for MRI images using 3D faster super-resolution convolutional neural network architecture. ITM Web Conf. 2020; 32:03044. https://doi.org/10.1051/itmconf/20203203044.

[18] Chen Y, Lin Z, Zhao X, Wang G, Gu Y. Deep learning-based classification of hyperspectral data. IEEE J. Sel. Top. Appl. Earth Obs. Remote Sens. 2014;7(6): 2094–107. https://doi.org/10.1109/JSTARS.2014.2329330.

[19] Kim J, Lee JK, Lee KM. Accurate image super-resolution using very deep convolutional networks. IEEE Comput Soc Conf Comput Vis Pattern Recog*n* 2016; 2016-Decem:1646–54. https://doi.org/10.1109/CVPR.2016.182.

[20] Ledig C, et al. Photo-realistic single image super-resolution using a generative adversarial network. in Proceedings - 30th IEEE Conference on Computer Vision and Pattern Recognition CVPR 2017;2017-Janua:105–14. https://doi.org/10.1109/CVPR.2017.19. Nov. 2017.

[21] Szegedy C, Ioffe S, Vanhoucke V, Alemi AA. Inception-v4, inception-ResNet and the impact of residual connections on learning. In: AAAI'17: Proceedings of the Thirty-First AAAI Conference on Artificial Intelligence; 2017. p. 4278–84.

[22] Mikolov T, Karafiát M, Burget L, Jan C, Khudanpur S. Recurrent neural network based language model. in Proceedings of the 11th Annual Conference of the International Speech Communication Association INTERSPEECH 2010:1045–8. 2010.

[23] Dong C, Loy CC, He K, Tang X. Learning a deep convolutional network for image super-resolution. in Lecture Notes in Computer Science (including subseries Lecture Notes in Artificial Intelligence and Lecture Notes in Bioinformatics) 2014; 8692:184–99. https://doi.org/10.1007/978-3-319-10593-2_13. LNCS, no. PART 4.

[24] Dong C, Loy CC, Tang X. Accelerating the super-resolution convolutional neural network. Lect Notes Comput Sci (including Subser Lect Notes Artif Intell Lect Notes Bioinformatics) Aug. 2016:391–407. Accessed: May 12, 2020. [Online]. Available: http://arxiv.org/abs/1608.00367.

[25] Kim J, Lee JK, Lee KM. Deeply-recursive convolutional network for image super-resolution. In *Proceedings of the IEEE conference on computer vision and pattern recognition*. 2016. p. 1637–45.

[26] Chen Y, Xie Y, Zhou Z, Shi F, Christodoulou AG, Li D. Brain MRI super resolution using 3D deep densely connected neutral network. " *arXiv*, no. 1. 2018. p. 1–20.

[27] Q. Lyu, H. Shan, and G. Wang, "MRI super-resolution with ensemble learning and complementary priors," IEEE Trans. Comput. Imaging, vol. 6, pp. 615–624, Jan. 2020, doi: 10.1109/tci.2020.2964201.

[28] Du J, Wang L, Liu Y, Zhou Z, He Z, Jia Y. Brain MRI super-resolution using 3D dilated convolutional encoder-decoder network. IEEE Access 2020;8:18938–50. https://doi.org/10.1109/ACCESS.2020.2968395.

[29] Pu Y, et al. Variational autoencoder for deep learning of images, labels and captions. " *arXiv Prepr. arXiv1609.08976*. 2016.

[30] S. Park, H. M. Gach, S. Kim, S. J. Lee, and Y. Motai, "Autoencoder-inspired convolutional network-based super-resolution method in MRI," IEEE J. Transl. Eng. Heal. Med., vol. 9, 2021, doi: 10.1109/JTEHM.2021.3076152.

[31] Shao Z, Wang L, Wang Z, Deng J. Remote sensing image super-resolution using sparse representation and coupled sparse autoencoder. IEEE J. Sel. Top. Appl. Earth Obs. Remote Sens. Aug. 2019;12(8):2663–74. https://doi.org/10.1109/JSTARS.2019.2925456.

[32] Lopez-Martin M, Carro B, Sanchez-Esguevillas A, Lloret J. Conditional variational autoencoder for prediction and feature recovery applied to intrusion detection in IoT. Sensors Aug. 2017;17(9). https://doi.org/10.3390/s17091967. 1967.

[33] Wang S, Zhang L, Liang Y, Pan Q. Semi-coupled dictionary learning with applications to image super-resolution and photo-sketch synthesis. In *Proceedings of the IEEE computer society Conference on computer Vision and pattern recognition*. 2012. p. 2216–23. https://doi.org/10.1109/CVPR.2012.6247930.

[34] Yang CY, Yang MH. Fast direct super-resolution by simple functions. in *Proceedings of the IEEE International Conference on Computer Vision* 2013:561–8. https://doi.org/10.1109/ICCV.2013.75.

[35] Chang H, Yeung DY, Xiong Y. Super-resolution through neighbor embedding. IEEE Comput Soc Conf Comput Vis Pattern Recog*n* 2004;1. https://doi.org/10.1109/cvpr.2004.1315043.

[36] Z. Wang, A. C. Bovik, H. R. Sheikh, and E. P. Simoncelli, "Image quality assessment: from error visibility to structural similarity," IEEE Trans Image Process, vol. 13, no. 4, pp. 600–612, Apr. 2004, doi: 10.1109/TIP.2003.819861.

[37] Huang Y, Long Y. Super-resolution using neural networks based on the optimal recovery theory. J Comput Electron Dec. 2006;5(4):275–81. https://doi.org/10.1007/s10825-006-0145-z.

[38] Lim B, Son S, Kim H, Nah S, Lee KM. Enhanced deep residual networks for single image super-resolution. ". IEEE computer society conference on computer vision and pattern recognition workshops, 2017-July; 2017. p. 1132–40. https://doi.org/10.1109/CVPRW.2017.151.

[39] Huang H, He R, Sun Z, Tan T. Wavelet-srnet: a wavelet-based cnn for multi-scale face super resolution. In *Proceedings of the IEEE international Conference on computer vision*. 2017. p. 1689–97.

[40] He K, Zhang X, Ren S, Sun J. Deep residual learning for image recognition. IEEE Comput Soc Conf Comput Vis Pattern Recog*n* 2016;2016-Decem:770–8. https://doi.org/10.1109/CVPR.2016.90.

[41] Huang G, Liu Z, Van Der Maaten L, Weinberger KQ. Densely connected convolutional networks. In *Proceedings of the IEEE conference on computer vision and pattern recognition*. 2017. p. 4700–8.

[42] Tong T, Li G, Liu X, Gao Q. Image super-resolution using dense skip connections. in *Proceedings of the IEEE international conference on computer vision* 2017:4799–807.

[43] Zhang Y, Tian Y, Kong Y, Zhong B, Fu Y. Residual dense network for image super-resolution. In: Proceedings of the IEEE conference on computer vision and pattern recognition; 2018. p. 2472–81.

[44] Tai Y, Yang J, Liu X. Image super-resolution via deep recursive residual network. In: Proceedings of the IEEE conference on computer vision and pattern recognition; 2017. p. 3147–55.

[45] Bahrami K, Shi F, Rekik I, Shen D. Convolutional neural network for reconstruction of 7T-like images from 3T MRI using appearance and anatomical features. Lect Notes Comput Sci Oct. 2016:39–47. https://doi.org/10.1007/978-3-319-46976-8_5. 10008 LNCS.

[46] Chen Y, Xie Y, Zhou Z, Shi F, Christodoulou AG, Li D. Brain MRI super resolution using 3D deep densely connected neural networks. in Proceedings - International Symposium on Biomedical Imaging May 2018;2018-April:739–42. https://doi.org/10.1109/ISBI.2018.8363679.

[47] F. Özyurt, E. Sert, and D. Avcı, "An expert system for brain tumor detection: fuzzy C-means with super resolution and convolutional neural network with extreme learning machine," Med Hypotheses, vol. 134, p. 109433, Jan. 2020, doi: 10.1016/j.mehy.2019.109433.

[48] M. Ebner et al., "An automated framework for localization, segmentation and super-resolution reconstruction of fetal brain MRI," Neuroimage, vol. 206, p. 116324, Feb. 2020, doi: 10.1016/j.neuroimage.2019.116324.

[49] X. Zhao, Y. Zhang, T. Zhang, and X. Zou, "channel splitting network for single MR image super-resolution," IEEE Trans Image Process, vol. 28, no. 11, pp. 5649–5662, Nov. 2019, doi: 10.1109/TIP.2019.2921882.

[50] Li X, Orchard MT. Novel sequential error-concealment techniques using orientation adaptive interpolation. IEEE Trans Circ Syst Video Technol Oct. 2002;12(10): 857–64. https://doi.org/10.1109/TCSVT.2002.804882.

[51] Poobathy D, Chezian RM. "Edge detection operators: peak signal to noise ratio based comparison," *IJ Image*. Graph. Signal Process. 2014;6(10):55–61.
[52] pp. 961–974 Structural approaches to image quality assessment. Jan. 2005. https://doi.org/10.1016/B978-012119792-6/50119-4.
[53] Sheikh HR, Bovik AC, de Veciana G. An information fidelity criterion for image quality assessment using natural scene statistics. IEEE Trans Image Process Dec. 2005;14(12):2117–28. https://doi.org/10.1109/TIP.2005.859389.
[54] Menze BH, et al. The multimodal brain tumor image segmentation benchmark (BRATS). IEEE Trans Med Imag Oct. 2015;34(10):1993–2024. https://doi.org/10.1109/TMI.2014.2377694.
[55] Bakas S, et al. Identifying the best machine learning algorithms for brain tumor segmentation, progression assessment, and overall survival prediction in the BRATS challenge. Nov. 2018 Accessed: Aug. 09, 2021. [Online]. Available: http://arxiv.org/abs/1811.02629.
[56] Bakas S, et al. Advancing the Cancer Genome Atlas glioma MRI collections with expert segmentation labels and radiomic features. Sci. Data Sep. 2017;4. https://doi.org/10.1038/SDATA.2017.117.
[57] This link is available: "MRBrainS18 | Grand Challenge on MR Brain Segmentation at MICCAI 2018.", https://mrbrains18.isi.uu.nl/. accessed Jun. 13, 2021).
[58] Shi W, et al. Real-time single image and video super-resolution using an efficient sub-pixel convolutional neural network. Proceedings of the IEEE computer society conference on computer vision and pattern recognition, 2016-December; Dec. 2016. p. 1874–83. https://doi.org/10.1109/CVPR.2016.207.
[59] Shi F, Cheng J, Wang L, Yap P-T, Shen D. LRTV: MR image super-resolution with low-rank and total variation regularizations. IEEE Trans Med Imag 2015;34(12):2459–66.
[60] Manjn JV, Coup P, Buades A, Fonov V, Louis Collins D, Robles M. Non-local MRI upsampling. Med Image Anal Dec. 2010;14(6):784–92. https://doi.org/10.1016/j.media.2010.05.010.
[61] Pham C-H, et al. Multiscale brain MRI super-resolution using deep 3D convolutional networks. Comput Med Imag Graph 2019;77:101647.
[62] Zeng K, Zheng H, Cai C, Yang Y, Zhang K, Chen Z. Simultaneous single- and multi-contrast super-resolution for brain MRI images based on a convolutional neural network. Comput Biol Med Aug. 2018;99:133–41. https://doi.org/10.1016/j.compbiomed.2018.06.010.
[63] Han W, Chang S, Liu D, Yu M, Witbrock M, Huang TS. Image super-resolution via dual-state recurrent networks. In *Proceedings of the IEEE conference on computer vision and pattern recognition*. 2018. p. 1654–63.
[64] J. Jiang, X. Ma, C. Chen, T. Lu, Z. Wang, and J. Ma, "Single image super-resolution via locally regularized anchored neighborhood regression and nonlocal means," IEEE Trans Multimed, vol. 19, no. 1, pp. 15–26, Jan. 2017, doi: 10.1109/TMM.2016.2599145.
[65] J. Yang, J. Wright, T. S. Huang, and Y. Ma, "Image super-resolution via sparse representation," IEEE Trans Image Process, vol. 19, no. 11, pp. 2861–2873, Nov. 2010, doi: 10.1109/TIP.2010.2050625.
[66] Lai WS, Bin Huang J, Ahuja N, Yang MH. Deep laplacian pyramid networks for fast and accurate super-resolution. in Proceedings - 30th IEEE Conference on Computer Vision and Pattern Recognition CVPR 2017;2017-January:5835–43. https://doi.org/10.1109/CVPR.2017.618. Nov. 2017.